Influence of reflected waves from the back surface of thin solid-plate specimen on velocity measurements by line-focus-beam acoustic microscopy

doi: 10.1109/58.818771

Influence of Reflected Waves from the Back Surface of Thin Solid-Plate Specimen on Velocity Measurements by Line-Focus-Beam Acoustic Microscopy

Jun-ichi Kushibiki, *Member, IEEE*, Yuji Ohashi, and Mototaka Arakawa

***Abstract*—We investigated the velocity measurements of leaky surface acoustic waves (LSAW) by line-focus-beam (LFB) acoustic microscopy of thin specimens for which the waves reflected from the back surface of the specimen (back reflection) must be included in the measurement model. The influence of back reflection resulted in a serious problem in measurement accuracy of the apparent changes of measured velocities. Using several samples of thin synthetic silica glasses, the determination of LSAW velocity affected by the reflected waves and the relationship between the specimen thickness and the apparent velocity change with a periodic frequency interval in the frequency dependence of measured LSAW velocities are discussed in detail. Three useful methods for eliminating that influence are proposed and demonstrated: first, separating the radio frequency (RF) pulsed wave signal from the specimen surface and the pulses reflected from the back surface by reducing the RF pulse width; second, scattering acoustic waves from the roughened back surface; and third, taking the moving average of measured frequency characteristics of LSAW velocities. It is shown that, among these methods, the moving average method is the most useful and effective as a general means to eliminate the influence and to determine intrinsic velocity values because this method needs no specimen process and no system change, and the same conventional $V(z)$ curve measurement and analysis can be employed.**

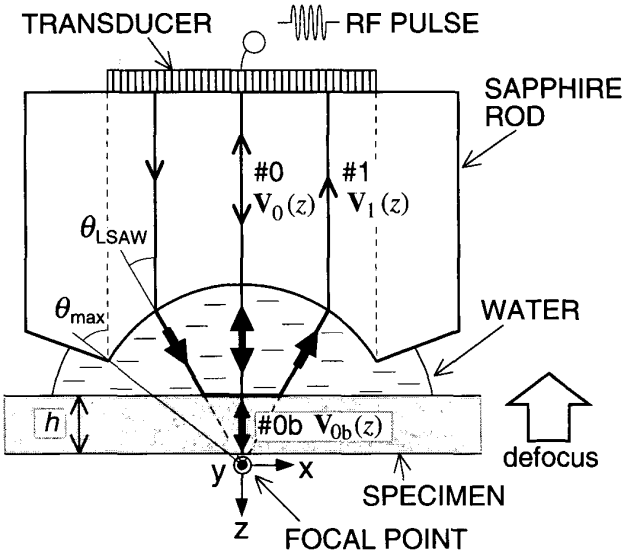

Fig. 1. Cross-section of the LFB acoustic lens describing $V(z)$ curve measurements.

I. Introduction

Line-focus-beam acoustic microscopy [1] has become recognized as a useful method of quantitative material characterization, which is made by measuring the propagation characteristics, i.e., velocity and attenuation, of LSAWs excited at the water-specimen interface through $V(z)$ curve measurements. This method has been applied to characterize a variety of materials [2]–[20], and its usefulness and effectiveness have been verified, resulting from the facts not only that the nondestructive and noncontacting measurement of acoustic properties can be conducted at a microscopic scale on a specimen surface over a large area, but also that the accuracy is extremely high. Temperature stability and mechanical precision on the measurement have been improved to the point that it has attained the relative accuracy in velocity of ±0.002%, at a chosen position, and of ±0.004% for two-dimensional (75 mm × 75 mm) inspection [21].

The propagation characteristics of LSAWs are obtained with the LFB system by measuring and analyzing the interference output $V(z)$ of two components: the waves reflected directly from the specimen surface and the reradiated waves of the LSAWs propagating on the boundary (see Fig. 1). The procedure of analysis of the $V(z)$ curves has been established based on the simple interference model of the two components [1]. However, this model is restricted to sufficiently thick specimens. As RF tone burst pulses are used in the measurement, another component, of which the waves are reflected from the back surface of the specimen (back reflection), takes part in the interference output in addition to the two components mentioned previously [22], [23]. If the specimen is thick enough, the component of back reflection has a sufficient time lag relative to the component of the waves reflected from the

Manuscript received August 2, 1999; accepted October 1, 1999. This work was supported in part by the Research Grant-in-Aids from the Ministry of Education, Science and Culture of Japan, the Japan Society for the Promotion of Science for the Research for the Future Program, and the Mitsubishi Foundation.

The authors are with the Department of Electrical Engineering, Tohoku University, Sendai 980-8579, Japan (e-mail: kushi@ecei.tohoku.ac.jp).

$$\mathbf{V}_0(z) = |\mathbf{V}_0(z)| \exp\{j(-2k_w z + \phi_0)\} \quad (1)$$

$$\mathbf{V}_1(z) = |\mathbf{V}_1(z)| \exp[j\{(-2k_w \cos\theta_{\mathrm{LSAW}})z + \phi_1\}], \text{ and} \quad (2)$$

$$\mathbf{V}_{0\mathrm{b}}(z) = \sum_n |\mathbf{V}_{0\mathrm{b}n}(z)| \exp\left\{j\left(-2k_w z - \frac{4n\pi fh}{V_\ell} + \phi_{0\mathrm{b}}\right)\right\} \quad (3)$$

specimen surface, such that the back reflection signals can be excluded by using a gate circuit in the system. However, if the specimen is thin, the back reflection component must be included in the output. As a result, the measured $V(z)$ curves are essentially affected, and the obtained LSAWs' propagation characteristics could be seriously affected.

In the previous studies, this influence has not been taken into consideration in the procedure because it could be assumed that the difference in acoustic impedance between water, as the coupling liquid, and the solid material, as the specimen, is significantly large so that the intensity of the wave component reflected from the back surface of the specimen is very small and its back-reflection effect is negligible because of the focusing of the acoustic beam. Now, however, the effect of the back reflection cannot be ignored as the measurement accuracy has been improved and the applications have been directed to greater accuracy required for detection of extremely small changes and profiles in the velocity of objects to be measured. It is of extreme importance that the effect of the back reflection on the measured values must be better known. In recent reports [22], [23], a measurement model to consider the back-reflection effects has been investigated, and a novel method of eliminating apparent velocity changes in measured values has been proposed and demonstrated.

In this paper, we investigate the effect on measurements of velocity using a plane wave model such that the back-reflection component, contributing to a transducer output, consists of only axial component waves as in synthetic silica (SiO_2) glasses. The relationships between the specimen thicknesses and measured velocity values are examined experimentally.

Next, we investigate the following three ways to exclude the influence on measured values. The first is the method for separating the pulsed wave signal reflected directly from the specimen surface and the pulsed wave signals reflected from the back surface by reducing the RF pulse width. The second is to scatter acoustic waves on the back surface by polishing the back surface of specimens roughly. The third is to apply the moving average method in the signal processing procedure to the frequency characteristics of LSAW velocities measured at a chosen position.

II. Measurement Model

Fig. 1 illustrates a cross-section of the LFB acoustic device with a specimen, which shows the formation principle of a $V(z)$ curve. When the specimen is thick, two components, $\mathbf{V}_0(z)$ and $\mathbf{V}_1(z)$, contribute to the transducer output. Such a thick specimen means that it is possible to separate the component of a pulsed wave reflected from the specimen surface and that of pulsed waves reflected from the back surface, in the time domain, and to consider the specimen as a semi-infinite medium when acoustic waves are excited by applying an RF tone burst pulse to the transducer. The measurement principle for this case was described in detail in [1]. Here, a more practical case of a thin specimen such as wafer-type substrates, used in electronic devices, is studied. In this case, the waves reflected from the back surface, $\mathbf{V}_{0\mathrm{b}}(z)$, are included in the transducer output in addition to the two components of $\mathbf{V}_0(z)$ and $\mathbf{V}_1(z)$ [22], [23]. It is assumed that the components of back reflection pass through only one #0b path as shown in Fig. 1. Supposing that the n-fold reflected component in the specimen is denoted as $\mathbf{V}_{0\mathrm{b}}n(z)$, each phaser is expressed as shown in (1)–(3), where $\theta_{\mathrm{LSAW}} = \sin^{-1}(V_w/V_{\mathrm{LSAW}})$, and V_w and V_ℓ are the longitudinal velocities of water and of the specimen, respectively; V_{LSAW} is the LSAW velocity; f is the ultrasonic frequency; h is the thickness of the specimen; and ϕ_0, ϕ_1, and $\phi_{0\mathrm{b}}$ are the initial phases. By moving the ultrasonic device toward the specimen (this operation is called 'defocus') and changing the relative distance z, the output $\mathbf{V}(z)$ curve is obtained as the sum of these three phasers given by the following equation:

$$\mathbf{V}(z) = \mathbf{V}_0(z) + \mathbf{V}_1(z) + \mathbf{V}_{0\mathrm{b}}(z). \quad (4)$$

The output of $\mathbf{V}(z)$ is approximately expressed as the scalar sum of the interference component, $V_I(z)$, and the component reflected directly from the specimen surface, $V_L(z)$, called the characteristic lens response [1]. As $V_L(z) = |\mathbf{V}_0(z)|$, subtracting $|\mathbf{V}_0(z)|$ from $\mathbf{V}(z)$ curve, ignoring the higher order terms, and using the conditions that $|\mathbf{V}_1(z)| \ll |\mathbf{V}_0(z)|$ and $|\mathbf{V}_{0\mathrm{b}n}(z)| \ll |\mathbf{V}_0(z)|$, the interference component $V_I(z)$ is expressed as

$$V_I(z) = |\mathbf{V}_1(z)| \cos\xi(z) + \sum_n \frac{|\mathbf{V}_{0\mathrm{b}n}(z)| \cdot |\mathbf{V}_1(z)|}{|\mathbf{V}_0(z)|} \cos\{\xi(z) + \mathcal{X}_n\} + \sum_n |\mathbf{V}_{0\mathrm{b}n}(z)| \cos\mathcal{X}_n \quad (5)$$

where

$$\xi(z) = 2k_w(1 - \cos\theta_{\mathrm{LSAW}})z + \phi_1 - \phi_0 \text{ and} \quad (6)$$

$$\mathcal{X}_n = \frac{4n\pi fh}{V_\ell} + \phi_0 - \phi_{0\mathrm{b}}. \quad (7)$$

If there is no back reflection $\mathbf{V}_{0b}(z)$, $V_I(z)$ is expressed by only the first term of (5), and the oscillation interval Δz and attenuation α_0 of the $V_I(z)$ curve are given as

$$\Delta z = \frac{\pi}{k_w\,(1-\cos\theta_{\mathrm{LSAW}})} \text{ and} \tag{8}$$

$$\alpha_0 = \frac{-2\alpha_w + 2\gamma\sin\theta_{\mathrm{LSAW}}}{\cos\theta_{\mathrm{LSAW}}} \tag{9}$$

where α_w and γ are the attenuation coefficients of longitudinal waves for water and of LSAWs, respectively. Then, the LSAW velocity and attenuation for a thick specimen are determined with Δz and α_0 through $V(z)$ curve analysis using the following relationships:

$$V_{\mathrm{LSAW}} = \frac{V_w}{\sqrt{1-\left(1-\frac{V_w}{2f\Delta z}\right)^2}} \text{ and} \tag{10}$$

$$\alpha_{\mathrm{LSAW}} = \frac{\gamma}{k_{\mathrm{LSAW}}} = \frac{\alpha_0\cdot\cos\theta_{\mathrm{LSAW}} + 2\alpha_w}{2k_{\mathrm{LSAW}}\cdot\sin\theta_{\mathrm{LSAW}}} \tag{11}$$

where k_{LSAW} is the wavenumber of the LSAWs.

When considering the back reflection, the 2nd and 3rd terms of (5) must be included, and the 2nd term changes the interference interval Δz and attenuation α_0. To make the effect clear, the interference component $V_I(z)$ can be transformed, omitting the 3rd term, and is expressed as follows:

$$V_I(z) \approx |\mathbf{V}_1(z)|\,\{1+\delta a_n(z)\}\cdot\cos\{\xi(z)+\delta p_n(z)\} \tag{12}$$

where

$$\delta a_n(z) = \frac{1}{|\mathbf{V}_0(z)|}\sum_n |\mathbf{V}_{0bn}(z)|\cos\mathcal{X}_n \text{ and} \tag{13}$$

$$\delta p_n(z) = \frac{1}{|\mathbf{V}_0(z)|\,\{1+\delta a_n(z)\}}\sum_n |\mathbf{V}_{0bn}(z)|\sin\mathcal{X}_n \approx \frac{1}{|\mathbf{V}_0(z)|}\sum_n |\mathbf{V}_{0bn}(z)|\sin\mathcal{X}_n. \tag{14}$$

Here, because $|\mathbf{V}_{0bn}(z)| \ll |\mathbf{V}_0(z)|$, $\delta a_n(z) \ll 1$, and $\delta p_n(z) \ll 1$, the approximations $\sin\delta p_n(z) \approx \delta p_n(z)$ and $\cos\delta p_n(z) \approx 1$ are used. In (12), the term $\cos\{\xi(z)+\delta p_n(z)\}$ contributes to the interference interval Δz, and the term $|\mathbf{V}_1(z)|\,\{1+\delta a_n(z)\}$ contributes to the attenuation α_0. From (12), the interference interval and attenuation of $V_I(z)$, denoted by $\Delta z'(z)$ and $\alpha_0'(z)$, are obtained as

$$\Delta z'(z) = \frac{\Delta z}{1+\frac{1}{2k_w(1-\cos\theta_{\mathrm{LSAW}})}\frac{\partial\delta p_n(z)}{\partial z}} \text{ and} \tag{15}$$

$$\alpha_0'(z) = \alpha_0 + \frac{1}{1+\delta a_n(z)}\frac{\partial\delta a_n(z)}{\partial z} \tag{16}$$

where $\Delta z'(z)$ and $\alpha_0'(z)$ are described as a function of z, and Δz and α_0 are given in (8) and (9), respectively. From (15) and (16), it is clear that $\Delta z'(z)$ and $\alpha_0'(z)$ are different from Δz and α_0 because of the terms $\delta p_n(z)$ and $\delta a_n(z)$. Thus, we examine the behavior of the terms $\delta p_n(z)$ and $\delta a_n(z)$ subsequently.

In (13) and (14), the terms $\delta a_n(z)$ and $\delta p_n(z)$ are related not only to $\mathcal{X}_n$ given in (7), but also to $|\mathbf{V}_0(z)|$ and $|\mathbf{V}_{0bn}(z)|$. When the specimen surface is located at the focus $z=0$, $|\mathbf{V}_0(z)|$ reaches its peak value because the wide spatial frequency components up to $\theta_{\max}$ are included in the transducer output and, when defocused, becomes a function of z, decreasing rapidly because the only low spatial frequency components near the axis, i.e., axial components, contribute to the transducer output because of the lens performance [1], [24]. On the other hand, when defocused, $|\mathbf{V}_{0bn}(z)|$ having only the axial component, is a function of z, increasing monotonically from the first assumption as the propagation attenuation in water decreases. Therefore, the function $|\mathbf{V}_{0bn}(z)|\,/\,|\mathbf{V}_0(z)|$ monotonically increases in the $-z$ direction, and the terms $\delta a_n(z)$ in (13) and $\delta p_n(z)$ in (14) exhibit monotonic increase or monotonic decrease, depending on the phase in the cosine and sine functions. According to the back-reflection effect, some changes in α_0 and Δz of the $V_I(z)$ curve occur depending on the differential coefficients of $\delta a_n(z)$ and $\delta p_n(z)$ with respect to z, as understood from (15) and (16), resulting in measurement errors of the LSAW phase velocity and attenuation. $\mathcal{X}_n$ is a function of the ultrasonic frequency f and the specimen thickness h as given by (7). Thus, in the frequency dependence of the propagation characteristics of velocity and attenuation, the differential coefficients of $\partial\delta a_n(z)/\partial z$ and $\partial\delta p_n(z)/\partial z$ at a fixed measurement position (with a constant h) vary periodically with f, just given in the form of the superposition of 1 to nth harmonics, where $\delta a_n(z)$ and $\delta p_n(z)$ are represented as summations of cosine and sine functions, respectively. When h is fixed, the frequency intervals ΔF_n for the n-fold back-reflection components are given as the frequency changes of 2π in (7) as

$$\Delta F_n = \frac{V_\ell}{2nh}, \quad (n=1,2,3,\ldots). \tag{17}$$

It can be understood from these expressions that the variations with the frequency interval ΔF_1 in the frequency domain, as a superposition of 1 to nth harmonic sinusoidal waves with the frequency intervals ΔF_n given by (17), are observed in the frequency dependence of LSAW velocity and attenuation.

Next, we discuss the condition in which the back reflection has no influence on the measured values of the LSAW velocities. Measurements of $V(z)$ curves are made using RF tone burst pulses, and the relationship between the specimen thickness h and the RF pulse width PW for the condition that $\mathbf{V}_0$ is not overlapped with $\mathbf{V}_{0b}$ in the time domain is given as

$$PW < \frac{2h}{V_\ell}. \tag{18}$$

For measurements around 200 MHz, we usually employ a cylindrical lens 1 mm in radius and a pulse width of about 500 ns. Here, the specimen thickness calculated for

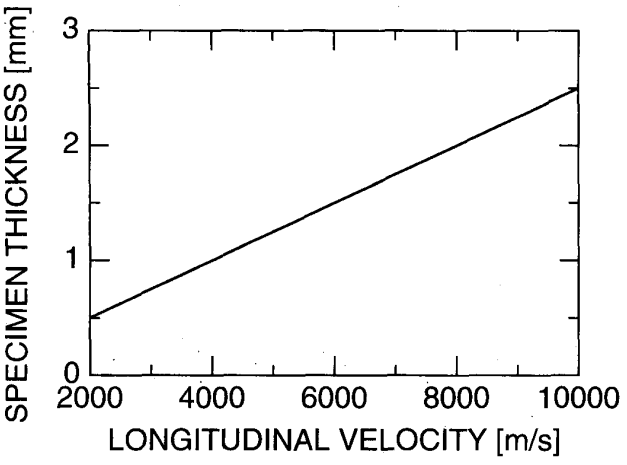

Fig. 2. Calculated result of the minimum specimen thickness h with no influence of the waves reflected from the back surface on the velocity measurement, using the equation $h = V_\ell \cdot PW/2$, where PW is the RF pulse width, 500 ns, and V_ℓ is the longitudinal velocity of material.

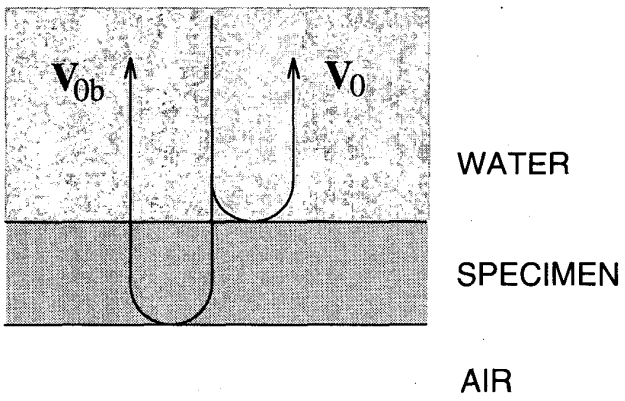

Fig. 3. Schematic diagram of longitudinal wave reflections at each boundary.

the condition that $PW = 500$ ns is shown in Fig. 2. The upper left side region of the solid line satisfies (18), in which ideal measurements can be conducted. In the lower right side region, the influence of the back reflection must be considered.

We now consider the amplitude of the waves because of the back reflection. The acoustic impedance and attenuation of the specimen should be taken into consideration as the parameters concerning its amplitude. The following simple model is used: the RF pulses of plane ultrasonic waves are normally incident on the water-specimen boundary, and a part of acoustic wave energy is transmitted into the specimen and is totally reflected from the specimen-air boundary as shown in Fig. 3. The reflection and transmission coefficients of the ultrasonic waves propagating from

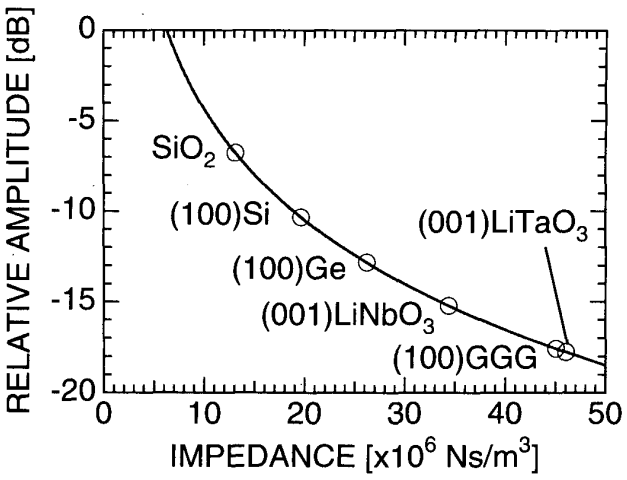

Fig. 4. Calculated result of the relative amplitude of longitudinal wave reflections from the back surface to that from the top surface as a function of acoustic impedance for several solid materials.

medium i to medium j, R_{ij} and T_{ij}, are given as follows:

$$R_{ij} = \frac{Z_j - Z_i}{Z_j + Z_i} \text{ and} \tag{19}$$

$$T_{ij} = \frac{2Z_j}{Z_j + Z_i} \tag{20}$$

where Z_i is the characteristic impedance of medium i. The amplitude of the waves reflected from the top surface, $|\mathbf{V}_0|$, and that from the back surface, $|\mathbf{V}_{0b}|$, are represented as

$$|\mathbf{V}_0| = |A \cdot R_{ws}| \text{ and} \tag{21}$$

$$|\mathbf{V}_{0b}| = |A \cdot T_{ws} \cdot R_{sa} \cdot T_{sw}| \tag{22}$$

where the subscripts w, s, and a denote water, specimen, and air, respectively. A is the amplitude of the incident wave at the water-specimen boundary. Here, the attenuation of the waves in the specimen is ignored because it is much smaller than that in water, and the propagation distance in the specimen is also shorter than that in water. It is assumed that the total reflection at the boundary between specimen and air occurs so that $R_{sa} = -1$. Therefore, $|\mathbf{V}_{0b}/\mathbf{V}_0|$ is given by

$$\left|\frac{\mathbf{V}_{0b}}{\mathbf{V}_0}\right| = \left|\frac{T_{ws} \cdot T_{sw}}{R_{ws}}\right|. \tag{23}$$

The calculated results for several typical solid materials are shown in Fig. 4 as a function of the acoustic impedance. It is seen from Fig. 4 that the relative amplitude decreases as the acoustic impedance increases. Therefore, less influence by the back reflection can be expected for solid materials with larger acoustic impedances. Although the situation for the focused waves is practically different from that for this model, that result could be a useful guide for consideration of the influence of back reflection. To investigate the influence of the back reflection in the following examination, synthetic silica glass with a relatively small acoustic

TABLE I
PREPARED SPECIMENS OF SYNTHETIC SILICA GLASS WITH VARIOUS THICKNESSES.

Sample	Thickness (mm)
1	0.2656
2	0.5786
3	1.0666
4	1.9648

impedance is taken as the specimen. This influence on the LSAW velocity, which is mainly adopted for material characterization, is investigated below.

III. INFLUENCE ON MEASURED LSAW VELOCITY

Four synthetic silica glass specimens (N-ES; Nippon Silica Glass Co., Tokyo, Japan) with various thicknesses shown in Table I were employed. All specimens have 30-mm diameters, and both of their surfaces are optically polished. The velocity of longitudinal waves is $V_\ell = 5928$ m/s, determined by the double-pulse interference method [25]. Thus, according to (18), $\mathbf{V}_0$ and $\mathbf{V}_{0b}$ do not overlap for the case of the specimens thicker than 1.5 mm, i.e., the thickness of sample 4 satisfies that condition.

To investigate how the back reflection influences the measured LSAW velocity, the frequency dependences of LSAW velocities for each specimen in Table I were measured in 1-MHz steps in the frequency range 120 to 270 MHz using the RF pulse width of 500 ns. Fig. 5 and 6 show typical $V(z)$ curves measured at 225 MHz and the final spectral distributions for samples 4 and 1 (see Table I). The dotted lines in Fig. 5(a) and 6(a) are the characteristic lens response $V_L(z)$. In both figures, it is clear that the two $V(z)$ curves differ from each other because of the back-reflection effect. Fig. 7 shows the results of the frequency dependence of LSAW velocities for samples 1 and 4 (see Table I). The frequency dependence for sample 4, shown by the solid line, is understood to be due mainly to the frequency characteristics of the LFB acoustic lens device [21] because the components of $\mathbf{V}_0$ and $\mathbf{V}_{0b}$ do not overlap. On the other hand, for sample 1, it can be interpreted that the dotted line involves the same frequency dependence as the solid line and the additional periodic change of about 10 MHz because the one- to five-fold components reflected from the back surface overlap with $\mathbf{V}_0$. So, by subtracting the solid line from the dotted line, in Fig. 7, the frequency dependence of the LFB device can be eliminated, and the curve in Fig. 8(a) is obtained. This figure shows the apparent velocity changes caused by the influence of the back reflection for sample 1. Similarly, the apparent velocity changes for samples 2 and 3 were obtained in Fig. 8(b) and (c), respectively. It is clear from Fig. 8 that the magnitude and frequency interval of the apparent velocity changes become smaller as the specimen thickness increases. Taking notice of the shape of the

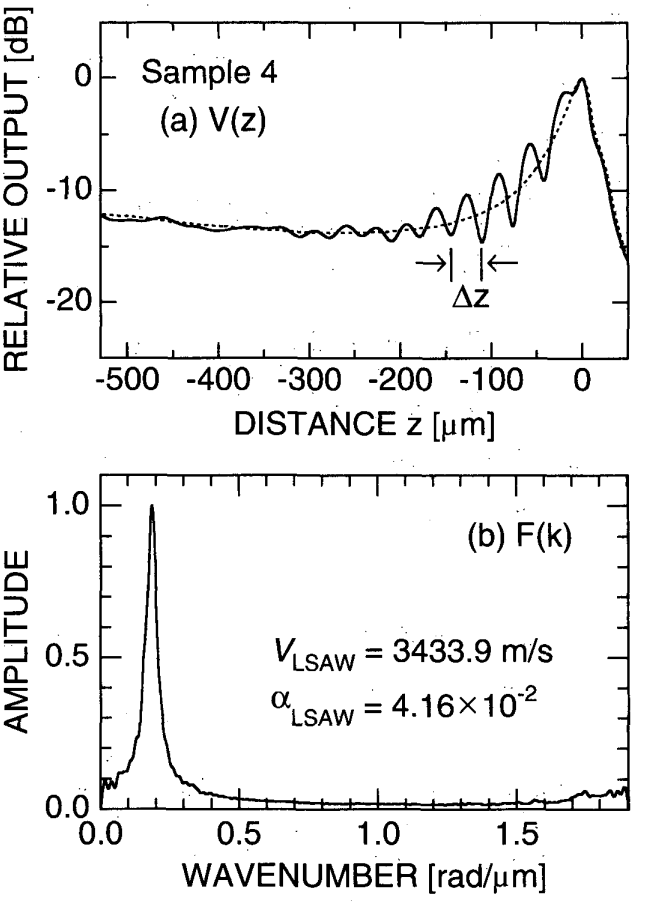

Fig. 5. $V(z)$ curve measured for sample 4 at 225 MHz with 500-ns pulse width (a) and spectral distribution obtained by $V(z)$ curve analysis (b). Dotted line in (a) is the characteristic lens response $V_L(z)$.

curves in Fig. 8, the curve in Fig. 8(a) exhibits a characteristic sharpened-upward curve in frequency dependence similar to a shape superposing several harmonic components because the one- to five-fold components reflected from the back surface contribute to the measurements. On the other hand, the curve in Fig. 8(c) is most likely sinusoidal in frequency dependence because only the one-fold component contributes to the measurements. The maximum deviations of the apparent LSAW velocity changes in the frequency range in Fig. 8 are 34.9 m/s (1.02%) for sample 1, 14.3 m/s (0.42%) for sample 2, and 5.3 m/s (0.15%) for sample 3.

Next, to discuss the frequency intervals in the periodic velocity change observed in Fig. 8, FFT analysis was carried out for each curve in Fig. 8. The result for the curve in Fig. 8(a) is shown in Fig. 9. Five peaks in the spectral distribution are detected, and the values are presented in Table II. In the same table, the calculated results obtained by substituting $V_\ell = 5928$ m/s and $n = 1 \sim 5$ into (17) are also given. These are in excellent agreement, within ± 0.02 MHz, and the number of the detected five peaks is also equal to the number of the fivefold components over-

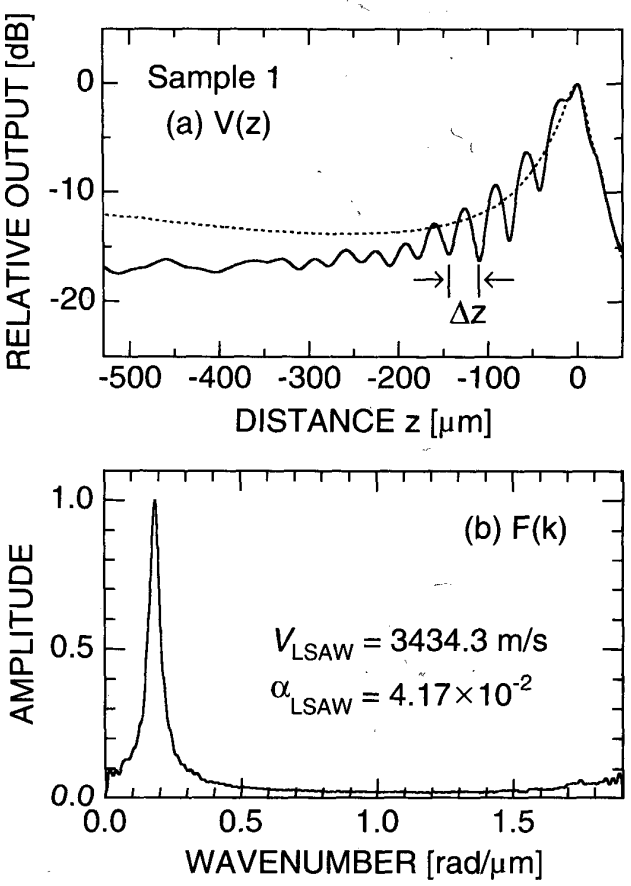

Fig. 6. $V(z)$ curve measured for sample 1 at 225 MHz with 500-ns pulse width (a) and spectral distribution obtained by $V(z)$ curve analysis (b). Dotted line in (a) is the characteristic lens response $V_L(z)$.

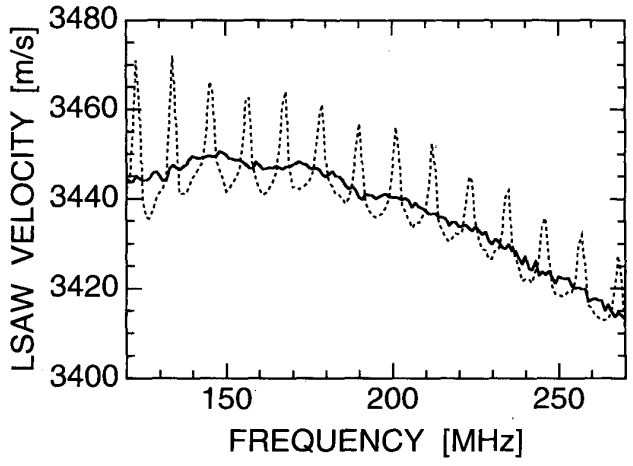

Fig. 7. Frequency dependences of LSAW velocities for SiO_2 glasses. Pulse width = 500 ns. Solid line: sample 4 with 1.9648-mm thickness; dotted line: sample 1 with 0.2656-mm thickness.

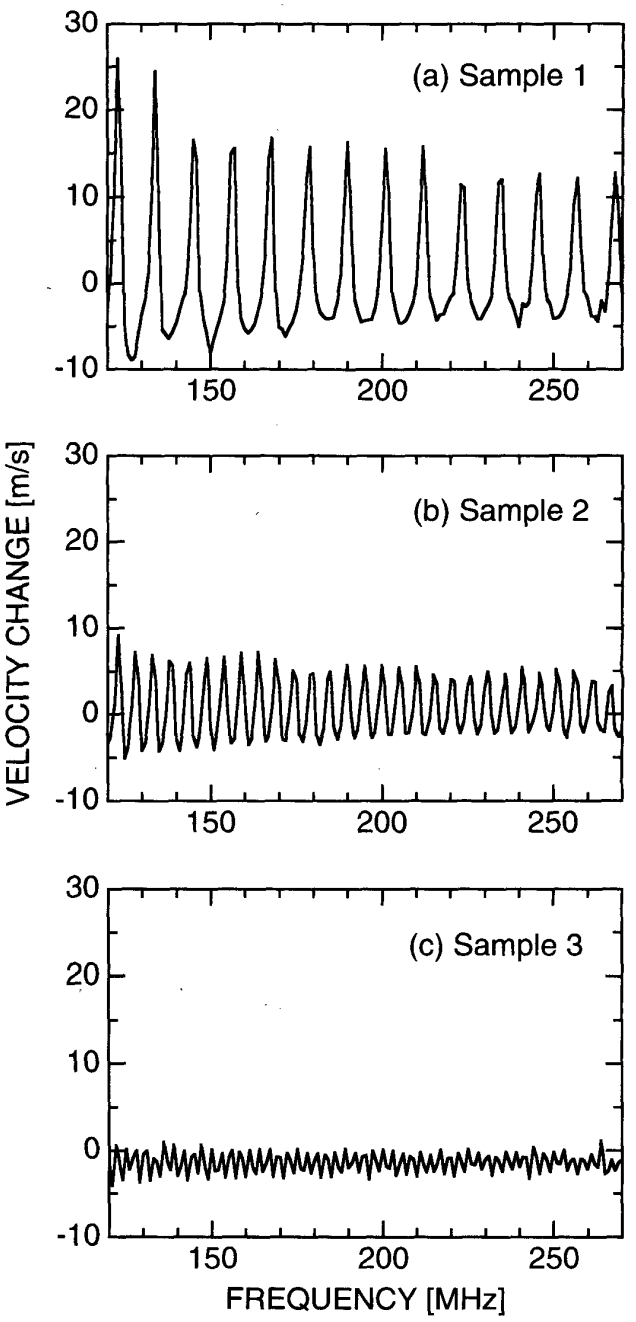

Fig. 8. Apparent LSAW velocity changes influenced by the waves reflected from the back surface of SiO_2 glass. Pulse width = 500 ns. Specimen thickness: (a) 0.2656 mm, (b) 0.5786 mm, and (c) 1.0666 mm.

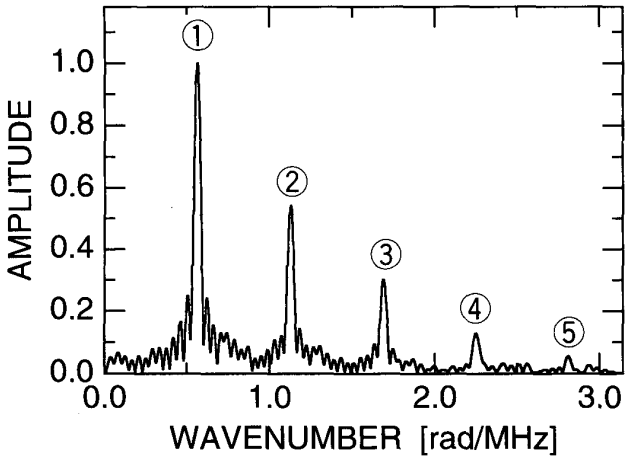

Fig. 9. Spectral distribution analyzed by FFT of the apparent LSAW velocity change in Fig. 8(a).

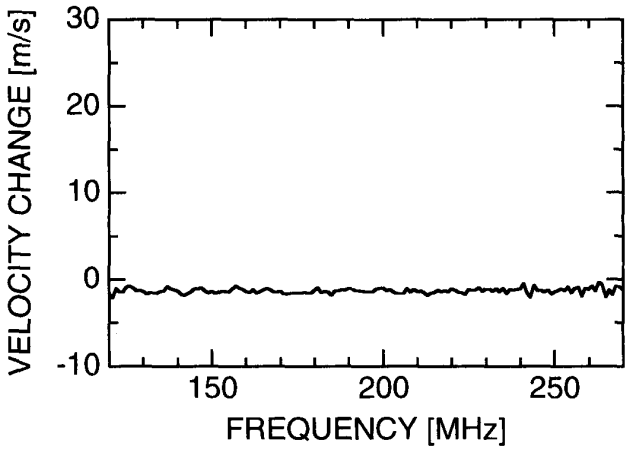

Fig. 10. LSAW velocity changes for sample 3 with 1.0666-mm thickness relative to the velocity values for sample 4 with 1.9648-mm thickness. Pulse width = 300 ns.

TABLE II
EXPERIMENTAL RESULTS OF SPECTRA SHOWN IN FIG. 9 AND CALCULATED RESULTS OF FREQUENCY INTERVALS OBTAINED BY (17).

No.	Measured (MHz)	Calculated (MHz)
1	11.183	11.160
2	5.574	5.580
3	3.717	3.720
4	2.791	2.790
5	2.236	2.232

lapped with $\mathbf{V}_0$, which is predicted for sample 1 with a 0.2656-mm thickness. In Table II, the frequency spectrum of the first peak can be regarded as the fundamental, and the following spectra correspond to the frequency intervals of the harmonic components. In a similar way, the measured frequency spectra of the first peak for Fig. 8(b) and (c) are 5.131 and 2.779 MHz, respectively, comparing favorably with the calculated values of 5.123 and 2.779 MHz. Further, the numbers of detected peaks are two for sample 2, 0.5786-mm thickness, and one for sample 3, 1.0666-mm thickness, which also corresponds to the numbers of the n-fold components overlapped with $\mathbf{V}_0$, that is $n = 2$ and 1, respectively. This shows that this simple model using plane waves is very useful for discussing the effect of the back reflection on the LSAW velocity. Therefore, it can be interpreted that the frequency intervals of the apparent and periodic velocity changes, shown in Fig. 8, are dominantly determined by ΔF_1 in (17).

IV. ELIMINATION METHODS

A. Pulse Width

The first way taken to eliminate the back reflection is to reduce the RF pulse width and separate the wave reflected directly from the specimen surface and the waves reflected from the back surface. For the two samples 3 and 4 of Table I, the frequency dependences of the LSAW velocities were measured using the pulse width of 300 ns, and the result for sample 3, by subtracting the frequency dependence of the LFB device measured for sample 4, is shown in Fig. 10. As shown in Fig. 8(c), which is the result obtained with the pulse width of 500 ns, the periodic changes were observed because the back reflection waves overlap with the front reflection waves $\mathbf{V}_0$ by 140 ns. In contrast, in Fig. 10, the back reflection waves are separated perfectly, and there is no periodic change. The maximum derivations of those apparent changes in LSAW velocity in Fig. 8(c) and Fig. 10 are 5.3 m/s (0.15%) and 1.8 m/s (0.052%), respectively. However, we consider that the variations of about 1.8 m/s in Fig. 10 are not due to the back-reflection effect but due to the accuracy of measurement for SiO_2, which is around $\pm 0.01\%$ for the shorter characterization distance z, -30 to -300 μm, because of higher attenuation of the relevant propagation wave mode caused by the water-loading effect on the SiO_2 substrate.

B. Scattering at the Back Surface

The second way is taken by scattering ultrasonic waves at the back surface roughened with grinding powder. The specimens were three synthetic silica glass specimens (T-4040; Toshiba Ceramics Co., Tokyo, Japan; dimensions: 30 mm × 25 mm × 0.5 mm) with the back surfaces roughened with the different grinding powders. The average particle diameters of the grinding powders are shown in Table III, in which the average roughnesses measured with the confocal laser scanning microscope (Leica Co., Heidelberg, Germany) are also given. The frequency characteristics of LSAW velocities are measured for those specimens with the pulse width of 500 ns, and the frequency characteristics of the LFB device is subtracted from each result. Fig. 11 shows the results of the apparent velocity changes

TABLE III
PARTICLE DIAMETER OF GRINDING POWDERS AND ROUGHNESS OF THE BACK SURFACE OF THE SPECIMEN.

Sample	Particle diameter (μm)	Roughness (μm)
A	0.5	0.3
B	40	1.4
C	80	2.2

for samples A, B, and C (Table III). In Fig. 11, the maximum deviations are 15.0 m/s (0.43%), 11.3 m/s (0.33%), and 7.9 m/s (0.23%), respectively, for samples A, B, and C. The longitudinal wavelength range in the synthetic silica glasses is 49.4 to 22.0 μm for the frequency range 120 to 270 MHz. As the wavelength becomes shorter relative to the roughness of the back surface, and, therefore, as the ultrasonic frequency becomes higher, the waves transmitted to the inside of the specimen are scattered more effectively at the back surface, and the apparent changes of LSAW velocity become smaller.

C. Moving Average

On the basis of the fact described in the previous section that the apparent changes of LSAW velocity can be represented as superposition of several harmonics, the third way can be taken to eliminate the apparent changes by taking the moving average processing of the frequency dependence of LSAW velocities. The moving average method is performed for the waveforms (a), (b), and (c) in Fig. 8 using the frequency intervals of 11, 5, and 3 MHz, which are determined to be the closest values to those obtained by FFT analysis. That processing was carried out two times in order to eliminate effectively the apparent changes. The solid lines in Fig. 12 are the obtained results; the dotted lines are the same as the solid lines in Fig. 8. The maximum deviations of the solid lines in Fig. 12 are 1.4 m/s (0.040%), 1.2 m/s (0.034%), and 0.8 m/s (0.024%), respectively, as the apparent velocity changes are eliminated effectively by the moving average processing, leaving only unavoidable variations associated with the accuracy of measurements. Furthermore, although the results of the moving average should appear around the line 0 m/s, basically if the same properties of the specimens were assumed, we see the slight differences obtained for each specimen within $\pm 1 \sim 2$ m/s, which suggests the significantly different properties among the specimens.

V. DISCUSSION

As observed in Fig. 8(c) and Fig. 10, the first method of reducing the RF pulse width is the easiest and most effective way for the specimens with lesser thicknesses that do not satisfy (18) for ideal measurements. However, considering that the thickness of most of the commercial wafers

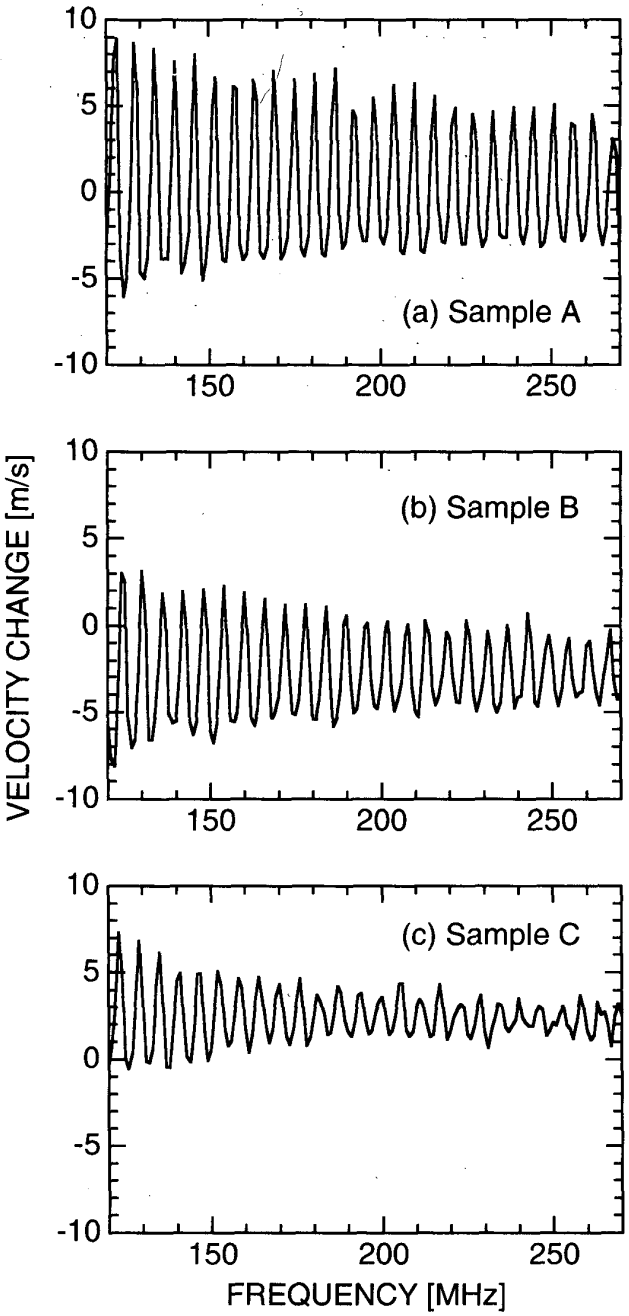

Fig. 11. Apparent LSAW velocity changes for the SiO_2 glasses with back surface roughened with various grinding powders. Pulse width = 500 ns. Grinding powder size: (a) 0.5 μm, (b) 40 μm, and (c) 80 μm.

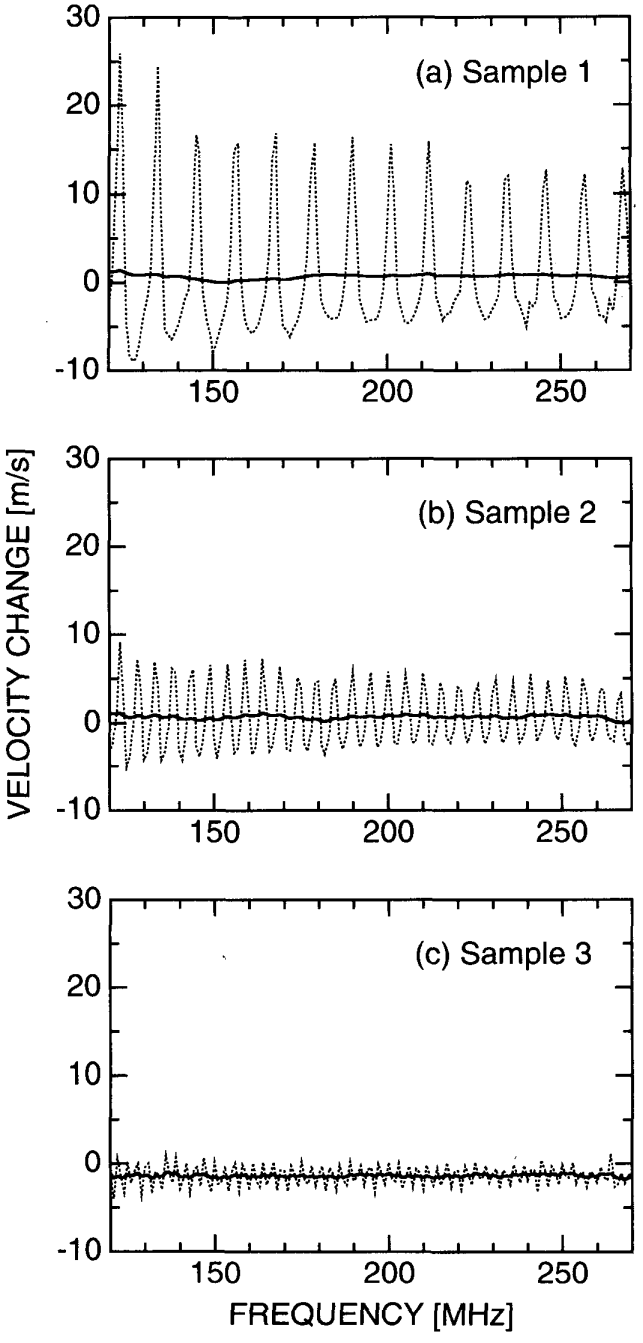

Fig. 12. Results obtained by a moving average processing for the waveforms shown by dotted lines.

for electronic devices is < 1 mm, this method is not always the best way to eliminate the influence of the back reflection for precise measurements. It can be understood from the results of Fig. 11 that the second method might be considerably more useful for the reduction of the back-reflection effect at higher frequencies, but it is also not an essential one for precise measurements.

As compared with the previous two methods, it can be said that the third method of moving average processing is the most useful of the three to eliminate the influence of back reflection because this method needs no specimen processing and no system change, and the same conventional $V(z)$ curve measurement and analysis can be employed.

To determine the LSAW velocities of the specimen, we may add the moving averaged value to the frequency dependence of LSAW velocities for sample 4 with no influence of the back reflection or we may apply the moving average processing directly to the measured frequency characteristics of LSAW velocities. For the purpose of obtaining the absolute LSAW velocity values, it is necessary to include the system calibration procedure using standard specimens [21] to eliminate the apparent frequency dependence of the LFB ultrasonic device. Obtaining the absolute value of LSAW velocity for sample 4 and adding the value to the averaged value of each solid line as shown in Fig. 12, we can, then, determine the true values of LSAW velocity for samples 1, 2, and 3, resulting in 3423.4, 3423.5, and 3421.4 m/s, respectively.

When measurements of one or two-dimensional scanning of LSAW velocity over a specimen surface are carried out, basically the true value at each measurement position can be obtained by measuring the frequency dependence of LSAW velocities at each measurement position and by taking those moving averages. However, this means that it takes a great deal of time to obtain the $V(z)$ curves and to process the curves. It is, therefore in the near future, necessary to develop some ideas for shortening the time for measurements.

VI. Conclusion

For material characterization by LFB acoustic microscopy, when the waves reflected from the back surface cannot be separated from the waves reflected from the top surface in the time domain because the specimen is thin, the influence of the back reflection on the measured LSAW velocities was investigated. It was confirmed by investigating the periodic frequency interval in the frequency dependence of LSAW velocities for SiO_2 glasses with different thicknesses that the vertical component waves of the back reflection, which are normally incident to the specimen surface, transmitted partially into the specimen, and reflected at the back surface, affect the determination of LSAW velocities. The condition of the specimen thickness with no influence on the back reflection was clarified. Then,

it was shown that the magnitude of the apparent changes of LSAW velocity depends on the thickness of the specimen and the ultrasonic frequency, and it was suggested that the magnitude also depends on the acoustic impedance of the specimens.

Then, for improvement, three methods of reducing the pulse width, scattering the back reflection, and taking the moving average processing of the frequency dependence of LSAW velocities were proposed, and their usefulness was studied experimentally. It was found that the moving average method is most useful. It became possible to apply the LFB system to precise characterization of thin specimens such as wafer-type substrates for which the influence of the back reflection cannot be eliminated simply by reducing the pulse width, without giving up measurement accuracy.

In this paper, we have taken synthetic silica glass as a specimen with a relatively small acoustic impedance for demonstration. However, we have already confirmed that the influences of the back reflection in measurements for $LiNbO_3$ and $LiTaO_3$ wafers with relatively large acoustic impedance exist. It is very important to consider the proper conditions, such as specimen thickness and RF pulse width, for precise measurements, as well as the system stability, such as mechanical precision and temperature stability [21], [26].

REFERENCES

[1] J. Kushibiki and N. Chubachi, "Material characterization by line-focus-beam acoustic microscope," *IEEE Trans. Sonics Ultrason.*, vol. SU-32, pp. 189–212, Mar. 1985.

[2] K. Yamanaka, J. Kushibiki, and N. Chubachi, "Anisotropy detection in hot-pressed silicon nitride by acoustic microscopy using the line-focus beam," *Electron. Lett.*, vol. 21, pp. 165–167, Feb. 1985.

[3] P. J. Burnett, G.A.D. Briggs, S. M. Al-Shukri, J. F. Duffy, and R. M. De La Rue, "Acoustic properties of proton-exchanged $LiNbO_3$ studied using the acoustic microscopy $V(z)$ technique," *J. Appl. Phys.*, vol. 60, pp. 2517–2522, Oct. 1986.

[4] J. Kushibiki, T. Ueda, and N. Chubachi, "Determination of elastic constants by LFB acoustic microscope," in *Proc. IEEE Ultrason. Symp.*, Denver, CO, pp. 817–821, 1987.

[5] C. K. Jen, C. Neron, J. F. Bussiere, L. Li, R. Lowe, and J. Kushibiki, "Characterization of cladded glass fibers using acoustic microscopy," *Appl. Phys. Lett.*, vol. 55, pp. 2485–2487, Dec. 1989.

[6] M. Obata, H. Shimada, and T. Mihara, "Stress dependence of leaky surface wave on PMMA by line-focus-beam acoustic microscope," *Exp. Mech.*, vol. 30, pp. 34–39, Mar. 1990.

[7] J. Kushibiki, T. Ishikawa, and N. Chubachi, "Cut-off characteristics of leaky Sezawa and pseudo-Sezawa wave modes for thin-film characterization," *Appl. Phys. Lett.*, vol. 57, pp. 1967–1969, Nov. 1990.

[8] J. Kushibiki, H. Takahashi, T. Kobayashi, and N. Chubachi, "Quantitative evaluation of elastic properties of $LiTaO_3$ crystals by line-focus-beam acoustic microscopy," *Appl. Phys. Lett.*, vol. 58, pp. 893–895, Mar. 1991.

[9] ——, "Characterization of $LiNbO_3$ crystals by line-focus-beam acoustic microscopy," *Appl. Phys. Lett.*, vol. 58, pp. 2622–2624, Jun. 1991.

[10] J. Kushibiki, T. Kobayashi, H. Ishiji, and N. Chubachi, "Elastic properties of 5-mol% MgO doped $LiNbO_3$ crystals measured by line focus beam acoustic microscopy," *Appl. Phys. Lett.*, vol. 61, pp. 2164–2166, Nov. 1992.

[11] C. K. Jen, Z. Wang, A. Nicolle, C. Neron, E. L. Adler, and J. Kushibiki, "Acoustic graded-index lenses," *Appl. Phys. Lett.*, vol. 59, pp. 1398–1400, Sep. 1991.

[12] T. Mihara and M. Obata, "Elastic constant measurement by using line-focus-beam acoustic microscope," *Exp. Mech.*, vol. 32, pp. 30–33, Mar. 1992.

[13] J. O. Kim, J. D. Achenbach, P. B. Mirkarimi, M. Shinn, and S. A. Barnett, "Elastic constants of single-crystal transition-metal nitride films measured by line-focus acoustic microscopy," *J. Appl. Phys.*, vol. 72, pp. 1805–1811, Sep. 1992.

[14] J. O. Kim, J. D. Achenbach, M. Shinn, and S. A. Barnett, "Effective elastic constants and acoustic properties of single-crystal TiN/NbN superlattices," *J. Mater. Res.*, vol. 7, pp. 2248–2256, Aug. 1992.

[15] C. K. Jen, C. Neron, A. Shang, K. Abe, L. Bonnell, and J. Kushibiki, "Acoustic characterization of silica glasses," *J. Amer. Ceram. Soc.*, vol. 76, pp. 712–716, Mar. 1993.

[16] Y. Ono, J. Kushibiki, and N. Chubachi, "Characterization of optical fiber preforms by line-focus-beam acoustic microscopy," in *Proc. IEEE Ultrason. Symp.*, Baltimore, MD, pp. 1243–1246, 1993.

[17] J. Kushibiki, H. Ishiji, T. Kobayashi, N. Chubachi, I. Sahashi, and T. Sasamata, "Characterization of 36°YX-$LiTaO_3$ wafers by line-focus-beam acoustic microscopy," *IEEE Trans. Ultrason., Ferroelect., Freq. Contr.*, vol. 42, pp. 83–90, Jan. 1995.

[18] Y.-C. Lee, J. O. Kim, and J. D. Achenbach, "Acoustic microscopy measurement of elastic constants and mass density," *IEEE Trans. Ultrason., Ferroelect., Freq. Contr.*, vol. 42, pp. 253–264, Mar. 1995.

[19] J. Kushibiki, M. Miyashita, and N. Chubachi, "Quantitative characterization of proton-exchanged layers in $LiTaO_3$ optoelectronic devices by line-focus-beam acoustic microscopy," *IEEE Photon. Technol. Lett.*, vol. 8, pp. 1516–1518, Nov. 1996.

[20] J. Kushibiki and M. Miyashita, "Characterization of domain-inverted layers in $LiTaO_3$ by line-focus-beam acoustic microscopy," *Jpn. J. Appl. Phys.*, vol. 36, pp. L959–L961, Jul. 1997.

[21] J. Kushibiki and M. Arakawa, "A method for calibrating the line-focus-beam acoustic microscopy system," *IEEE Trans. Ultrason., Ferroelect., Freq. Contr.*, vol. 45, pp. 421–430, Mar. 1998.

[22] J. Kushibiki, Y. Ohashi, and M. Arakawa, "Precise velocity measurements for thin specimens by line-focus-beam acoustic microscopy," *Jpn. J. Appl. Phys.*, vol. 38, pp. L89–L91, Jan. 1999.

[23] J. Kushibiki and Y. Ohashi, "Theoretical and experimental considerations on line-focus-beam acoustic microscopy for thin specimens," *Jpn. J. Appl. Phys.*, vol. 38, pp. L342–L344, Mar. 1999.

[24] W. Parmon and H. L. Bertoni, "Ray interpretation of the material signature in the acoustic microscope," *Electron. Lett.*, vol. 15, pp. 684–686, Oct. 1979.

[25] J. Kushibiki, T. Wakahara, T. Kobayashi, and N. Chubachi, "A calibration method of the LFB acoustic microscope system using isotropic standard specimens," in *Proc. IEEE Ultrason. Symp.*, Tucson, AZ, pp. 719–722, 1992.

[26] T. Kobayashi, J. Kushibiki, and N. Chubachi, "Improvement of measurement accuracy of line-focus-beam acoustic microscope system," in *Proc. IEEE Ultrason. Symp.*, Tucson, AZ, pp. 739–742, 1992.

Jun-ichi Kushibiki (M'83) was born in Hirosaki, Japan, on November 23, 1947. He received the B.S., M.S., and Ph.D. degrees in electrical engineering from Tohoku University, Sendai, Japan, in 1971, 1973, and 1976, respectively.

In 1976, he became Research Associate at the Research Institute of Electrical Communication, Tohoku University. In 1979, he joined the Department of Electrical Engineering, Faculty of Engineering, Tohoku University, where he was Associate Professor from 1988 to 1993 and became Professor in 1994. He has been studying ultrasonic metrology, especially acoustic microscopy and its applications, and has established a method of material characterization by LFB acoustic microscopy. He also has been interested in biological

tissue characterization in the higher frequency range, applying both bulk and acoustic microscopy techniques.

Dr. Kushibiki is a member of the Acoustical Society of America; the Institute of Electronics, Information, and Communication Engineers of Japan; the Institute of Electrical Engineers of Japan; the Acoustical Society of Japan; and the Japan Society of Ultrasonics in Medicine.

Yuji Ohashi was born in Toyama Prefecture, Japan, on August 27, 1973. He received the B.S. and M.S. degrees in electrical engineering from Tohoku University, Sendai, Japan, in 1996 and 1999, respectively.

He is currently studying toward the Ph.D. degree at Tohoku University. His research interests include development of LFB acoustic microscopy system and its applications to materials characterization.

Mr. Ohashi is a member of the Acoustical Society of Japan.

Mototaka Arakawa was born in Sendai, Japan, on January 19, 1971. He received the B.S. and M.S. degrees in electrical engineering from Tohoku University, Sendai, Japan, in 1993 and 1995, respectively.

He is currently studying toward the Ph.D. degree at Tohoku University. His research interests include developments of the measurement methods of elastic constants of solid materials and of the calibration method of the LFB acoustic microscopy system.

Mr. Arakawa is a member of the Acoustical Society of Japan and the Institute of Electronics, Information, and Communication Engineers of Japan.